Experimental Neurology 223 (2010) 385–393

Contents lists available at ScienceDirect

Experimental Neurology

journal homepage: www.elsevier.com/locate/yexnr

Structural and functional changes in tau mutant mice neurons are not linked to the presence of NFTs

A.B. Rocher [a], J.L. Crimins [a], J.M. Amatrudo [a], M.S. Kinson [a], M.A. Todd-Brown [a], J. Lewis [b], J.I. Luebke [a,*]

[a] Department of Anatomy and Neurobiology, M949, Boston University School of Medicine, 85 E. Newton St., Boston, MA 02118, USA
[b] Department of Neuroscience, Mayo Clinic, Jacksonville, FL, USA

ARTICLE INFO

Article history:
Received 25 March 2009
Revised 10 July 2009
Accepted 24 July 2009
Available online 7 August 2009

Keywords:
Patch clamp
In vitro slice
Dendrite
Dendritic spine
Tauopathy
FTDP-17
Alzheimer's disease
Transgenic model
Frontal
Pyramidal cell

ABSTRACT

In the rTg4510 mouse model, expression of the mutant human tau variant P301L leads to development of neurofibrillary tangles (NFTs), neuronal death, and memory impairment, reminiscent of the pathology observed in human tauopathies. In the present study, we examined the effects of mutant tau expression on the electrophysiology and morphology of individual neurons using whole-cell patch-clamp recordings and biocytin filling of pyramidal cells in cortical slices prepared from rTg4510 (TG) and wild-type (WT) littermate mice. Among the TG cells, 42% contained a clear Thioflavin-S positive inclusion in the soma and were categorized as NFT positive (NFT+), while 58% had no discernable inclusion and were categorized as NFT negative (NFT−). The resting membrane potential (V_r) was significantly depolarized (+8 mV) in TG cells, and as a consequence, evoked repetitive action potential (AP) firing rates were also significantly increased. Further, single APs were significantly shorter in duration in TG cells and the depolarizing voltage deflection or "sag" evoked by hyperpolarization was significantly greater in amplitude. In addition to these functional electrophysiological changes, TG cells exhibited significant morphological alterations, including loss or significant atrophy of the apical tuft, reduced dendritic complexity and length, and reduced spine density. Importantly, NFT− and NFT+ TG cells were indistinguishable with regard to both morphological and electrophysiological properties. Our observations show that expression of mutated tau results in significant structural and functional changes in neurons, but that these changes occur independent of mature NFT formation.

Introduction

The microtubule-associated protein tau plays a key role in stabilization and assembly of microtubules, which are critical for the maintenance of normal cellular morphology and cellular trafficking. Neurodegenerative tauopathies are characterized by abnormal intracellular accumulations of fibrillar tau, termed neurofibrillary tangles (NFTs), which can result from mutation of the tau gene (e.g. frontotemporal dementia and parkinsonism linked to chromosome 17; FTDP-17), mutation of other disease-related genes such as the one encoding amyloid precursor protein (e.g. Alzheimer's Disease), or from currently undefined mechanisms (review: Lee et al., 2001; Ballatore et al., 2007). Tau mutations result in decreased binding of tau to microtubules, resulting in destabilization of microtubules; unbound tau then develops a propensity to hyperphosphorylate, recompartmentalize from the axon to the soma and dendrites, and aggregate in the form of NFTs. The P301L mutation of tau is commonly seen in FTDP-17 (Poorkaj et al., 2001), and the conditional mouse model rTg4510 that expresses the P301L mutation closely mimics features of human tauopathies including progressive NFT deposition, widespread neuron death, and memory impairment (Santacruz et al., 2005).

Studies examining the relationship between tau and neuronal death in specific brain regions have resulted in varying conclusions regarding the role that NFTs versus soluble non-fibrillar species play in neurodegeneration (review: Bretteville and Planel, 2008; Congdon and Duff, 2008; Spires-Jones et al., 2009). The number of NFTs has been positively correlated with the progression of neurodegeneration and dementia in AD (Lee et al., 2001) leading to the widely-held assumption that NFTs are neurotoxic. However, data from several studies suggest a possibly neutral, if not outright protective, role for NFTs (Bussière et al., 2003; Bretteville and Planel, 2008; Congdon and Duff, 2008). For example, in mice that overexpress wild-type human tau, extensive neuronal death occurred prior to substantial deposition of aggregated tau and NFTs, and neurons that appeared to be dying exhibited no ultrastructural evidence of fibrillar tau (Andorfer et al., 2005). Similarly, it has been demonstrated that NFTs and neuronal death are not associated in the hippocampus, cortex, or striatum of the rTg4510 mouse model (Spires et al., 2006). While these studies have assessed the relationship of NFTs to neuronal death, information regarding the effect of NFTs and of soluble non-fibrillar tau on the structure and function of individual neurons is lacking. Since tau

* Corresponding author. Fax: +1 617 638 5954.
E-mail address: jluebke@bu.edu (J.I. Luebke).

0014-4886/$ – see front matter © 2009 Elsevier Inc. All rights reserved.
doi:10.1016/j.expneurol.2009.07.029

interacts with a wide array of structural and functional proteins, mutations in tau that lead to NFT deposition could be expected to significantly alter neuronal structure and function without necessarily being lethal to a given neuron. Because cellular morphology is a primary determinant of neuronal firing patterns and synaptic integration, it is logical to further hypothesize that any tau-related morphological changes may lead to alterations in functional electrophysiological properties which, in turn, could impact neuronal network properties in a given brain area. In the present study, the effects of tau mutation on the structure and function of individual frontal cortical neurons in rTg4510 versus wild-type mice were assessed for the first time.

Materials and methods

Experimental subjects

Studies were performed using six rTg(tau_{P301L})4510 (TG) and six age-matched wild-type (WT) mice that were 8.5 months of age. Mice were screened for activator and responder transgenes (Santacruz et al., 2005) using a standardized PCR assay for tail DNA. All mice were given *ad libitum* access to food and water. Animal care and experiments were conducted in accordance with standards set forth by the National Institutes of Health Guide for the Care and Use of Laboratory Animals and the United States Public Health Service Policy on Humane Care and Use of Laboratory Animals. The Mayo Clinic and the Boston University Institutional Animal Care and Use Committees (IACUC) approved all animal procedures.

Slice preparation

Mice were sacrificed by decapitation and their brains were rapidly removed and submerged in oxygenated (95% O_2 and 5% CO_2) ice-cold Ringer's solution, concentrations (in mM): 25 $NaHCO_3$, 124 NaCl, 1 KCl, 2 KH_2PO_4, 10 Glucose, 2.5 $CaCl_2$, and 1.3 $MgCl_2$, (pH 7.4; Sigma-Aldrich, St. Louis, MO). Post-extraction, dissected cortical hemispheres were affixed to an agar slab with cyanoacrylate glue and placed in a tissue holder for cutting. Eight to 10 coronal slices (300 μm thick) of the rostral third of the brain were cut into ice-cold Ringer's solution with a vibrating microtome. Following cutting, slices were equilibrated for a minimum of 1 h at room temperature (RT) in oxygenated Ringer's solution. For recording, individual slices were positioned in submersion-type recording chambers (Harvard Apparatus, Holliston, MA) on Nikon E600 infrared-differential interference contrast microscope (IR-DIC; Micro Video Instruments, Avon, MA) stages and were continuously perfused with RT oxygenated Ringer's solution (2–2.5 ml/min).

Whole-cell patch-clamp recordings

Whole-cell patch-clamp recordings were obtained from individual layer 3 frontal cortical pyramidal cells which were identified under IR-DIC optics. For assessment of electrophysiological properties, recordings were conducted as previously described (Chang and Luebke, 2007; Chang et al., 2005). Patch electrode pipettes pulled from capillary tubes on a Flaming and Brown horizontal pipette puller (Model P87, Sutter Instrument, Novato, CA) were filled with potassium methanesulfonate internal solution, concentrations (in mM): 122 KCH_3SO_3, 2 $MgCl_2$, 5 EGTA, and 10 NaHEPES containing 1% biocytin (pH 7.4; Sigma-Aldrich, St. Louis, MO). In Ringer's solution, pipettes had a resistance of between 3 and 6 MΩ. "PatchMaster" acquisition software (HEKA Elektronik, Lambrecht, Germany) was used for data acquisition with EPC-9 and EPC-10 amplifiers (HEKA Elektronik). Signals were low-pass filtered at 10 kHz. Cells were maintained at resting membrane potential during current-clamp recordings.

Passive membrane properties and action potential (AP) firing properties

Resting membrane potential (V_r), input resistance (R_n) and membrane time constant were determined in current-clamp mode. V_r was determined as the voltage recorded in the absence of current injection. R_n was calculated as the slope of a best-fit line through a voltage–current relationship plot of steady-state voltage responses to 9 successive 10 pA current steps (−40 to +40 pA), 200 ms in duration. Membrane time constant was determined by fitting a single-exponential function to the first 100 ms of a 200 ms, 20 pA hyperpolarizing current step. Single AP property measurements were performed on the first AP generated in a 200 ms current-clamp series. These properties included AP threshold, amplitude, and duration at half amplitude. The rheobase (minimum current required to evoke a single AP), was determined with a 10 s depolarizing current ramp from 0–200 pA using the FitMaster software (HEKA Elektronik) measuring tool. AP firing threshold was measured on an expanded time scale at the initiation of the sharp upward spike deflection. AP amplitude was calculated from the threshold to the peak of the spike and duration at half amplitude of the AP. A series of 12 hyperpolarizing and depolarizing current steps (in 50 pA increments from −170 to +380 pA), each 2 s in duration, was implemented for evaluation of repetitive AP firing. Characteristic of an I_h mediated depolarization (Zhang et al., 2006), the 2 s −170 pA hyperpolarizing current step evoked a slowly emergent depolarizing voltage "sag". "Sag" amplitude was measured from the minimum voltage to the maximum amplitude of deflection toward depolarization using the FitMaster software measuring tool. FitMaster software event detection was used for determination of AP frequency.

Slice processing and confocal scanning

During recording (~15 min/cell), cells were simultaneously filled with biocytin. Slices were then promptly placed in a 4% paraformaldehyde in 0.1 M phosphate buffered saline (PBS) solution (pH 7.4). Following overnight fixation at 4 °C, slices were rinsed in PBS (3 times, 10 min each) and placed in 0.1% Triton X-100/PBS for 2 h at RT. Slices were then incubated in streptavidin–Alexa 546 (1:500; InVitrogen, Carlsbad, CA) at 4 °C for 48 h. For visualization of neurofibrillary tangles (NFTs) slices from both groups (WT and TG) were incubated in 0.01% Thioflavin-S. Thioflavin-S staining is a sensitive method conventionally employed for the post-mortem detection of NFTs in brains from patients with tauopathy (e.g. Sun et al., 2002; Santa-Maria et al., 2006) and from animal models of tauopathy (review: Lewis and Hutton, 2005). Following mounting with Prolong Gold mounting medium (InVitrogen) and coverslipping, stained slices were scanned with a Zeiss 510 confocal laser-scanning microscope using a Plan-Apochromat 40×/1.3 NA oil objective lens (210 μm working-distance). For localization of NFTs in somata, fluorescence emitted by Alexa-546 (Helium/Neon laser excitation) and Thioflavin-S (Argon laser excitation) were collected in two channels with 560 nm and 480–520 nm pass filters respectively. Each "soma stack" was acquired at a resolution of 0.1×0.1×0.5 μm per voxel (Fig. 1). For dendritic reconstructions, two to three stacks per cell were obtained using a voxel size of 0.4×0.4×0.41 μm. Approximately 10 stacks per cell, each with a field of view of 153 μm^2, were acquired at a very high resolution for spine analyses (5 cells per group). These stacks were captured using a 0.1×0.1×0.2 μm voxel size.

Data processing and three-dimensional (3D) morphologic analyses

Pre-processing of image stacks

Each image stack was deconvolved using Autodeblur software (Media Cybernetics, Bethesda, MD) to reduce signal blurring. With Volume Integration and Alignment System (VIAS) software (Rodriguez et al., 2003), deconvolved stacks were aligned in 3D and

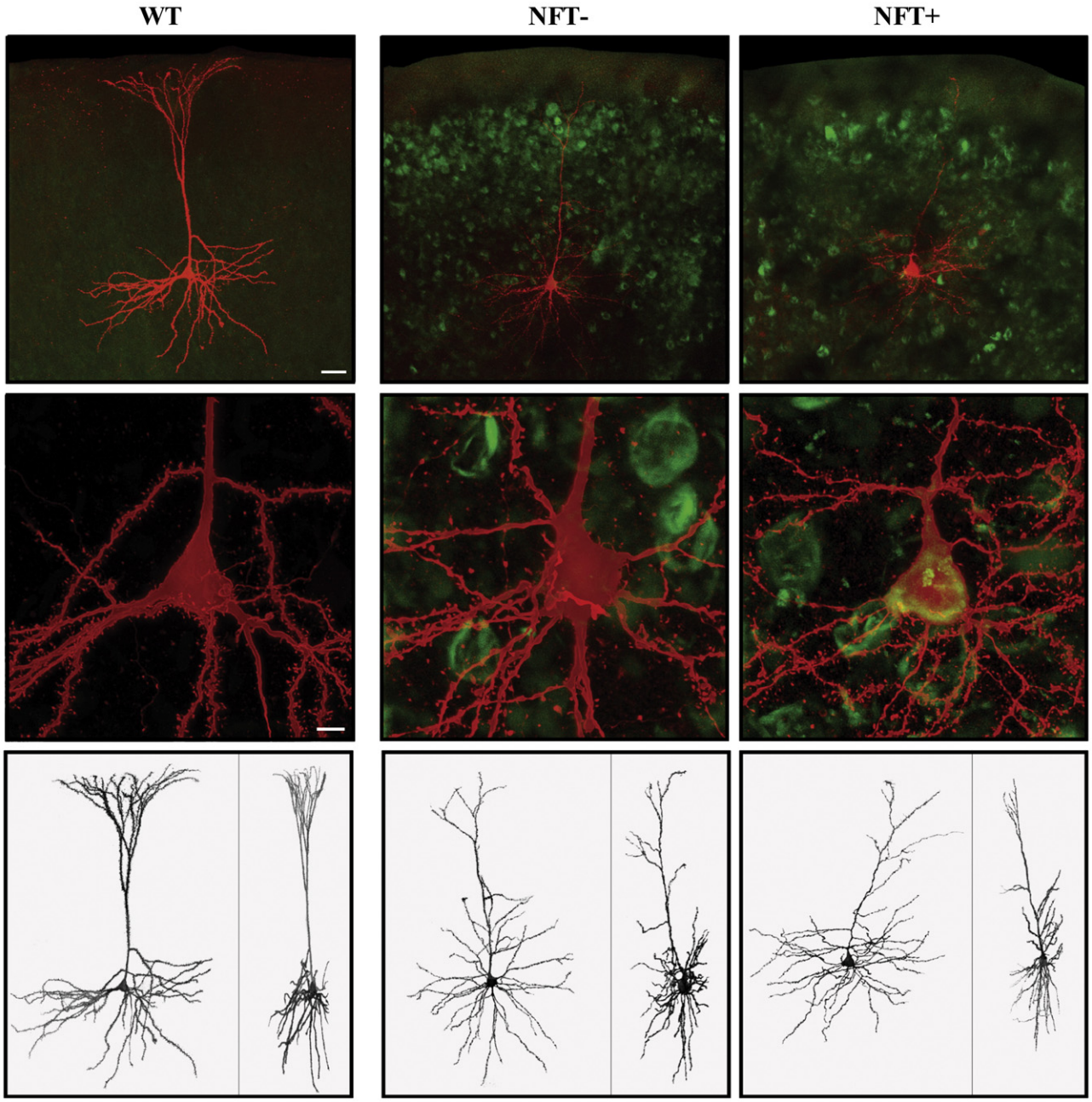

Fig. 1. Confocal images of representative streptavidin–Alexa 546-labeled layer 3 pyramidal cells from WT (left) and TG (center and right) mice. Top row: low magnification confocal images of the cells with Thioflavin-S staining showing a high density of NFTs in the cortex of TG mice. Middle row: Somata of cells shown in top row at higher magnification. Imaging the Thioflavin-S staining in the soma allows for the classification of the TG cells into one of 2 groups based on the absence or presence of an NFT, respectively named NFT− cells (center column) and NFT+ cells (right column). Bottom row: 3D reconstruction of cells imaged at high resolution (xy and xz projections on the left and right sides of each panel, respectively). Scale bars: top row = 40 μm; middle row = 5 μm.

subsequently integrated into a single volumetric dataset. Using the VIAS measure tool, distance to the soma from the pial surface, the vertical extent of the basal and apical arbors (including the tuft), and the horizontal extent of the basal arbor, the apical arbor (without the tuft), and the apical tuft were determined.

Morphometric analyses of somata and dendrites

For automatic 3D cell reconstruction designed for analyses of somatic and dendritic parameters, single volumetric datasets (obtained from VIAS) were imported into AutoNeuron software (MBF Bioscience, Williston, VT). Reconstruction data were then exported to companion NeuroExplorer software (MBF Bioscience, Williston, VT). Morphological parameters of dendrites included length (μm), number of bifurcation nodes (indicative of complexity), and surface area (μm^2). Surface area was also calculated for the somata. Length and number of bifurcation nodes were assessed for total (apical and basal dendritic arbors combined) dendritic expanses, and for both the apical (normalized to distance from pial surface measurements) and basal arbors using a Sholl analysis (Sholl, 1953). For Sholl analyses, basal and apical arbors were divided separately by length into proximal, middle, and distal thirds based upon the total extent of the arbor in consideration.

Spine detection and analyses

Dendritic spines were detected using the 64-bit version of NeuronStudio (Wearne et al., 2005; available at: http://www.mssm.

Table 1
Electrophysiological properties.

	WT	TG	NFT−	NFT+
Passive membrane properties				
Membrane time constant (ms)	32.5 ± 4.1	35.2 ± 3.4	36.5 ± 4.6	33.4 ± 5.3
Input resistance (MOhm)	197 ± 23	228 ± 23	257 ± 35	189 ± 28
Membrane resting potential (mV)	−74.9 ± 1.1	−67.0 ± 1.1***	−67.6 ± 1.6	−66.2 ± 1.6
Single AP properties				
Rheobase (mA)	92 ± 14	73 ± 7	66 ± 8	81 ± 14
Threshold (mV)	−35.8 ± 0.5	−34.8 ± 1.7	−34.4 ± 2.7	−35.5 ± 1.8
Amplitude (pA)	86.3 ± 0.9	84.3 ± 1.3	82.8 ± 1.4	86.3 ± 2.5
Duration (ms)	1.42 ± 0.05	1.25 ± 0.05*	1.30 ± 0.06	1.19 ± 0.07
Sag amplitude (mV)	2.23 ± 0.46	5.94 ± 0.62***	5.76 ± 0.90	5.54 ± 0.93

WT versus TG.
*$p<0.02$; ***$p<0.0001$.

edu/cnic) on the full-resolution stacks produced by VIAS integration. Using NeuronStudio the entire dendritic structure of each cell was automatically traced and subsequently dendritic spines were detected automatically by the program around the traced dendrites using a Rayburst-based spine analysis routine (Rodriguez et al., 2003, 2006; Radley et al., 2008). Dendritic spine detection was performed on the entire apical dendritic arbor and a single basilar dendritic branch. An operator then inspected each cell and made corrections as needed using the NeuronStudio interface.

Cell inclusion criteria

Cells included in analyses were required to meet both electrophysiological and morphological criteria. Electrophysiological criteria were: a resting membrane potential of ≤ −55 mV (or a holding current of <100 pA at −70 mV), stable access resistance, an AP overshoot, and ability to fire repetitive APs during prolonged depolarizing current steps. Morphological criteria were: an intact soma; a completely filled dendritic arbor with no cut dendrites in the proximal third of the apical dendritic arbor and, for TG cells, unequivocal labeling with Thioflavin-S to enable classification of the cells as NFT+ or NFT−.

Statistical analyses

The two-tailed Student's *t*-test was used to compare electrophysiological and morphological data for WT versus TG and NFT+ versus NFT− cells. Relationships between electrophysiological variables (that differed significantly between the WT and TG groups) and morphological variables were examined with linear regression analyses (Pearson product–moment correlation). Null hypotheses were rejected with a p-value ≤ 0.05. All data are presented as the mean plus or minus the standard error of the mean (SEM). Detailed electrophysiological and high-resolution morphological analyses of fifty-six cells (11 NFT+, 15 NFT−, and 30 WT) were performed in this study. This number was adequate for performing statistical analyses and for drawing meaningful conclusions regarding differences in both electrophysiological and morphological properties of cells from rTg4510 mice compared to those from aged-matched wild-type mice. This is because first, there was a low degree of within-group variability in the data and second, between-group comparisons revealed robust, statistically significant differences between transgenic and wild-type neurons (Tables 1 and 2).

Results

A total of 26 TG and 30 WT cells met both electrophysiological and morphological criteria for inclusion in this study. Among the TG cells, 42% contained a clear Thioflavin-S positive inclusion in the soma and were categorized as neurofibrillary tangle positive (NFT+), while 58% had no discernable Thioflavin-S label and were categorized as NFT negative (NFT−). Representative WT, NFT−, and NFT+ cells are shown in Fig. 1.

TG cells exhibit a significantly depolarized resting membrane potential and increased action potential (AP) firing rates in response to depolarizing current steps

There was no difference in mean input resistance (R_n) or mean membrane time constant between TG and WT cells (Table 1). However, TG cells exhibited a significantly depolarized (by a mean of +8 mV) resting membrane potential (V_r) compared to WT cells ($p<0.0001$, Table 1). Within the TG group, there was no difference in R_n, membrane time constant, or V_r between NFT− and NFT+ cells (Table 1).

Single AP properties did not differ between TG and WT cells with regard to mean rheobase, threshold, or amplitude, but the mean duration was significantly decreased in TG cells ($p<0.02$;

Table 2
Morphological properties.

		WT	TG	NFT−	NFT+
Dendrites and somata					
Distance of soma from pial surface (μm)		340 ± 13	372 ± 17	388 ± 24	351 ± 26
Soma surface area (μm²)		730 ± 46	842 ± 50	799 ± 62	901 ± 86
Vertical extent (μm)	Basal dendrites	195 ± 9	170 ± 11	164 ± 15	178 ± 18
	Apical dendrite	316 ± 12	340 ± 22	355 ± 29	321 ± 33
Horizontal extent (μm)	Basal dendrites	294 ± 10	307 ± 15	326 ± 21	282 ± 19
	Apical dendrite	255 ± 11	261 ± 16	267 ± 24	79 ± 13
	Apical tuft	253 ± 18	173 ± 23**	183 ± 34	159 ± 28
Diameter (μm)	Basal dendrites	1.26 ± 0.02	1.23 ± 0.02	1.23 ± 0.03	1.23 ± 0.03
	Apical dendrite	1.32 ± 0.02	1.31 ± 0.02	1.31 ± 0.03	1.30 ± 0.03
Total cell surface area (μm²)		21,919 ± 971	19,296 ± 1292	18,765 ± 1903	20,019 ± 1800
Dendritic spines					
Spine density (spines/μm)	Basal dendrite	1.36 ± 0.17	0.84 ± 0.12*	0.66 ± 0.10	1.01 ± 0.19
	Apical dendrite	1.10 ± 0.08	0.79 ± 0.16*	0.79 ± 0.06	0.78 ± 0.09

WT versus TG.
*$p<0.02$; **$p<0.01$.

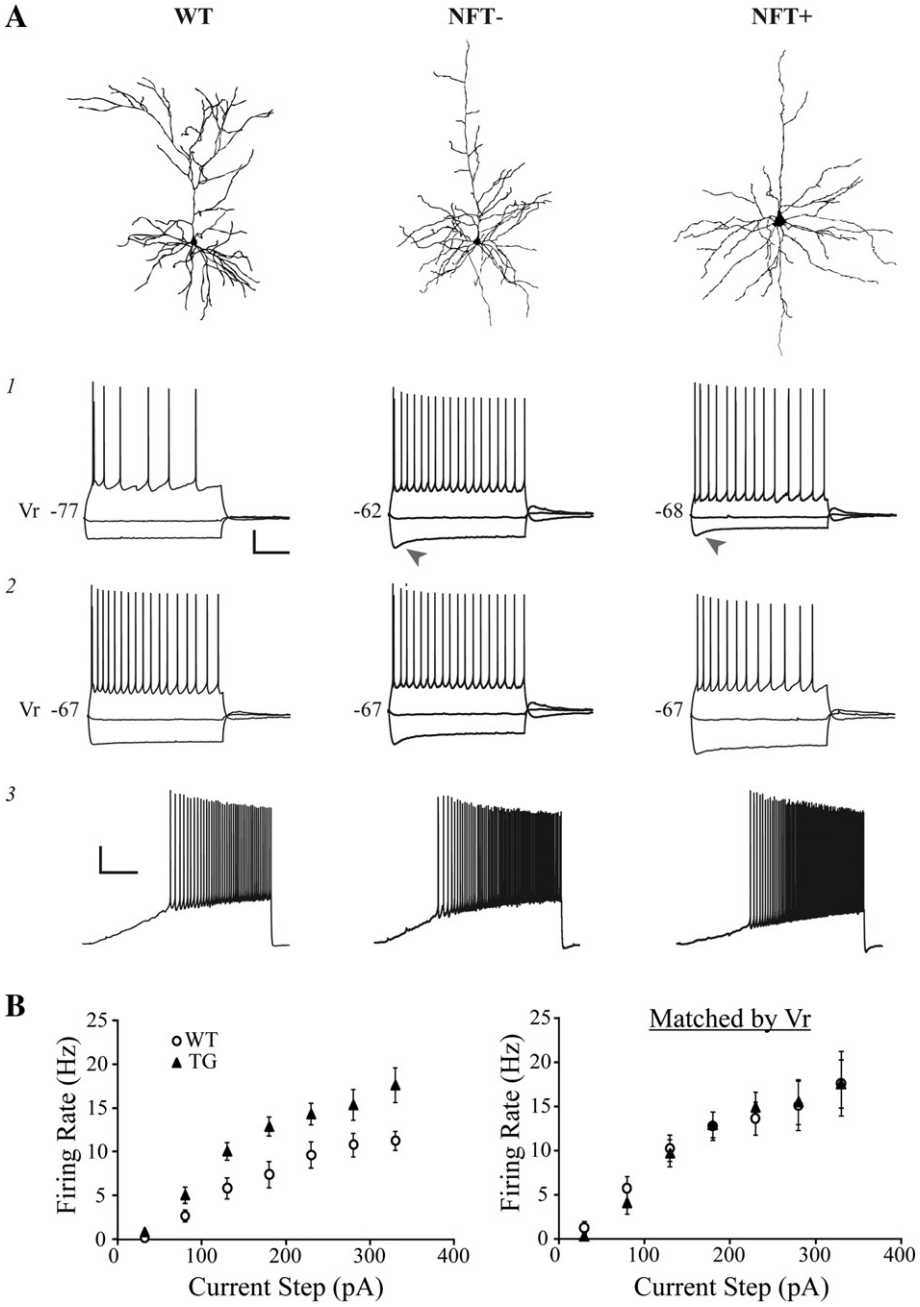

Fig. 2. Membrane voltage responses to injected current from representative WT, NFT− and NFT+ cells. A) Top: cells from which recordings shown in panels A1 and 3 were obtained. Panels 1–3: Membrane voltage responses evoked by 2 s current steps in cells with different V_r (1), and in cells matched by V_r (2), or by a 10 s depolarizing current ramp from 0 to 200 pA (3). WT cells fired at a lower frequency than either NFT− or NFT+ cells while the latter two groups did not differ (1). Arrowheads indicate a pronounced "sag" in TG (but not WT) cells. None of the groups differed significantly in firing frequency when matched by V_r (2). Scale bars: 1 and 2 = 20 mV, 500 ms; 3 = 20 mV, 2 s. B) Mean frequency–current plots for all WT and TG cells (left, $p<0.05$ at each current step) and for subgroups of WT and TG cells that are matched by V_r (right).

Table 1). A series of 2 s hyperpolarizing and depolarizing current steps were applied to each cell to elicit voltage responses. Strong hyperpolarizing current steps elicited a non-linear depolarizing voltage deflection or "sag" that was significantly greater in TG compared to WT cells ($p<0.0001$; Table 1; Fig. 2A_1, arrowheads). The mean AP firing rate (FR) elicited from resting membrane potential by increasing amplitude depolarizing current steps was significantly higher in TG compared to WT cells (Fig. 2). This increase in FR of TG cells ranged from 42% to 90% depending upon the amount of depolarizing current injected during 2 s steps, but was significantly greater at every step ($p<0.05$; Fig. 2B, left). Action potential FR was dependent on V_r (not shown; Pearson product–moment correlation between V_r and FR at the +230 pA step: $R=0.520$; $p<0.0001$), and when TG and WT cells were held at the same membrane potential (e.g. −67 mV as in Fig. 2A_2) identical depolarizing steps elicited a comparable number of APs in both groups. Similarly, when depolarizing steps were administered to TG and WT cells that had the same V_r identical FRs were obtained (Fig. 2B, right). It was thus demonstrated that the increase in FR of TG cells is due to a substantially depolarized V_r. Within the TG group the NFT− and NFT+ cells did not differ with regard to mean single AP properties, sag amplitude, or FR (Table 1, Fig. 2).

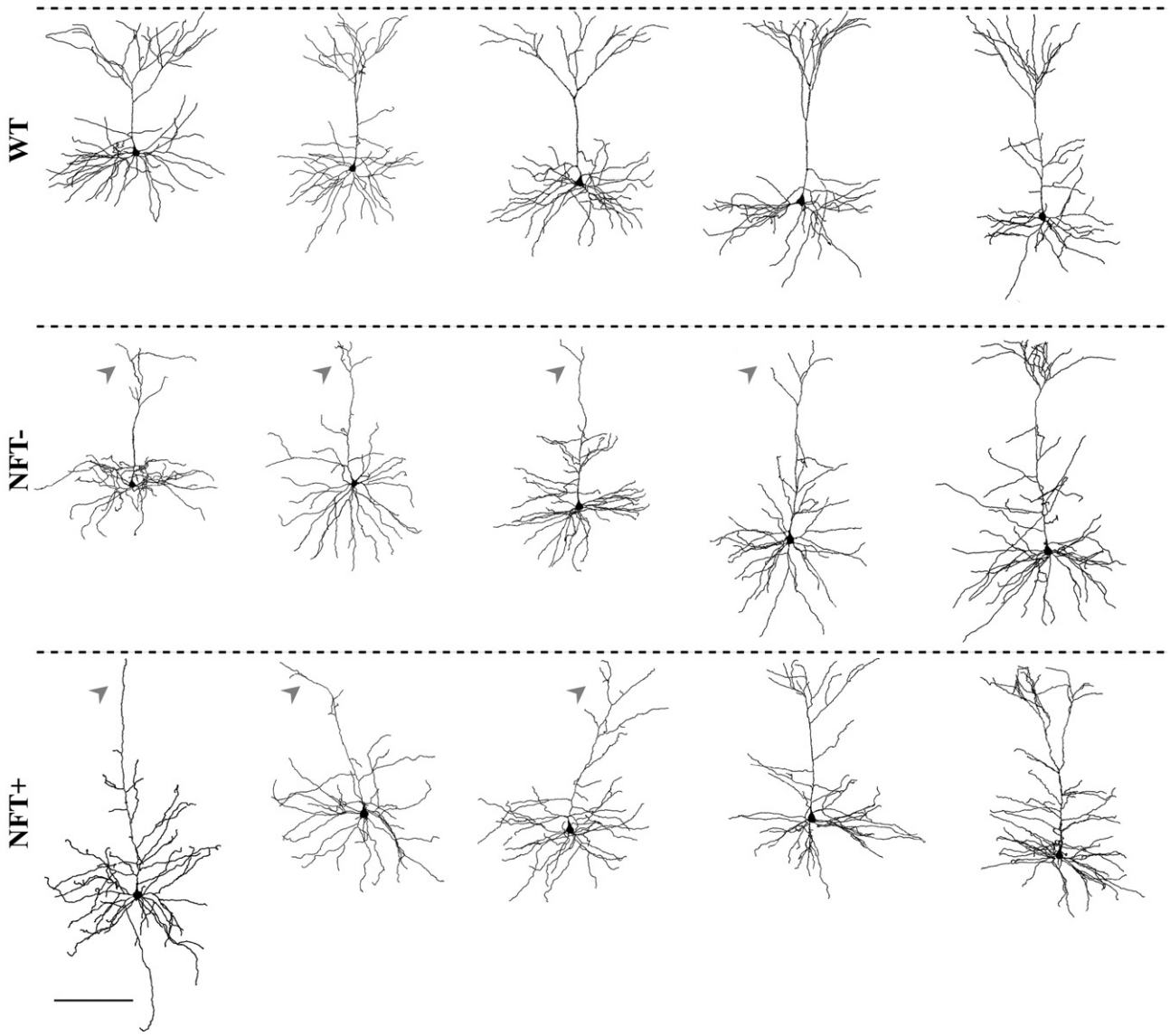

Fig. 3. Reconstructions of representative cells from WT and TG mice showing morphological diversity. Fully reconstructed WT (top), NFT− (middle) and NFT+ (bottom) frontal cortical pyramidal cells. Dashed lines indicate the pial surface. Arrowheads indicate severe apical tuft atrophy. Scale bar = 200 μm.

Atrophy of the apical dendritic tuft occurs in a large proportion of TG cells

Detailed morphological analyses were performed on all electrophysiologically characterized cells. The mean distance of the somata from the pial surface was not significantly different between TG and WT cells (Table 2) and all were clearly identifiable as layer 3 pyramidal cells.

In initial analyses, the following general morphological properties of the dendritic arbors of TG and WT cells were assessed: total cell surface area, surface area of the soma, vertical and horizontal extents of the basal and apical dendritic arbors, and mean horizontal extent of the apical dendritic tuft. These properties did not differ between TG and WT cells, with the notable exception of a significantly reduced mean horizontal extent of the apical tuft in the TG group ($p<0.006$; Table 2). The majority (65%) of TG cells displayed severe apical tuft atrophy, such that in the distal-most part of the arbor the dendrite was either not branched or sparsely branched (Fig. 3, arrowheads). The remaining TG cells (35%) retained an apical tuft which was indistinguishable from those seen in WT cells (Fig. 3). Importantly, apical tuft atrophy was not associated with the presence or absence of NFTs in TG cells (Fig. 3). In addition, within the TG group there was no difference in general morphological characteristics between NFT− and NFT+ cells (Table 2).

Significant alterations in dendritic length and complexity in TG cells

Assessment of the length and complexity (number of bifurcation nodes) of apical and basal dendritic arbors revealed significant differences between TG and WT cells (Fig. 4).

As shown in Fig. 4, Sholl analyses revealed circumscribed reductions in complexity and length of the dendritic arbors of TG cells. The mean number of nodes was significantly lower in the middle third of the apical arbor in TG compared to WT cells ($p<0.05$). There was also a clear trend toward a reduced number of nodes in the distal third of the apical arbor although this did not achieve statistical significance ($p<0.06$). In the basal arbors of TG cells there was a significant reduction in the number of nodes in the proximal and middle thirds of the arbor ($p<0.03$). Sholl analyses also revealed that in TG cells there was a significant reduction in the total length of dendritic segments in the distal third of the apical dendritic arbor ($p<0.002$) while the total lengths of segments in the proximal and

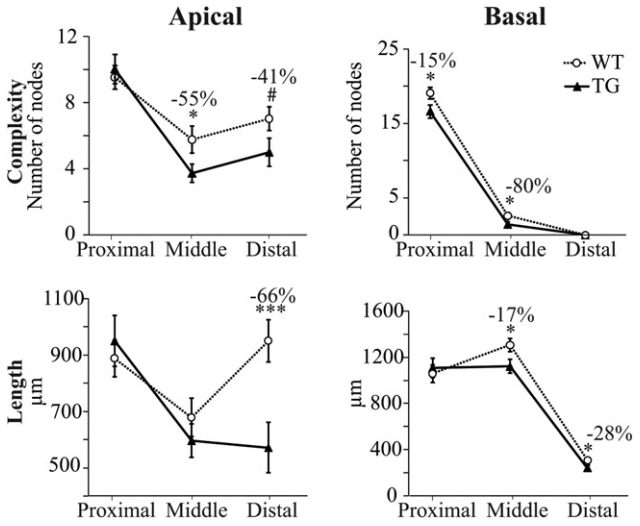

Fig. 4. Significant alterations in the length and complexity of apical and basal dendritic arbors of TG cells. Proximal, middle, and distal thirds of the dendritic arbors were examined. Complexity, as reflected by the number of bifurcation nodes (top), and total length (bottom) are plotted for the apical (left) and basal (right) dendritic arbors of WT and TG cells. Note, in particular the dramatic decrease (−66%) in length in the distal third of the apical arbor of TG cells. #$p = 0.06$; *$p < 0.05$; ***$p < 0.002$.

middle thirds were not significantly reduced. The total length of the basal arbor was significantly reduced in the middle ($p < 0.02$) and distal thirds ($p < 0.03$) in the TG cells. Within the TG cells there was no difference in the complexity or length of the apical and basal dendritic arbors between NFT− and NFT+ cells.

Qualitative dendritic diameter changes in TG cells

Upon qualitative examination, reduction in dendritic diameter was apparent for many TG cells (e.g. Figs. 1 and 5). However, quantitative assessment of diameter did not reveal a difference between the TG and WT nor between NFT− and NFT+ cells within the TG group. This is likely due to the fact that dendrites of cells in the TG group often exhibited constrictions and swellings along their arbors (Fig. 5) making it difficult to accurately assess dendritic diameter in these cells. In addition, the degree of dendritic thinning, while marked in some branches of some TG cells, was not apparent in all branches of a given cell nor in all TG cells; this large degree of variability precluded quantitative demonstration of reduced dendritic diameter in the TG cells.

Significant reduction in dendritic spine density in TG cells

Dendritic spine density was significantly reduced in both the apical and the basal dendritic arbors of TG cells (−29% and −38% respectively, $p \leq 0.02$; Fig. 5). Within the TG group, density of dendritic spines did not differ between NFT− and NFT+ cells (Table 2). Fig. 5 depicts apical dendritic branches from representative WT, NFT− and NFT+ cells. In addition to the clear loss of dendritic spines, there were changes in the distribution of morphological subtypes of spines, with an apparent loss of thin, stubby and mushroom type spines and an increase in the number of long, thin filopodia-type spines.

Relationship between morphological and electrophysiological changes in TG cells

In order to determine whether specific morphological changes were related to electrophysiological changes, we performed Pearson product–moment correlations between morphological variables and each electrophysiological variable that was significantly altered in the TG cells (V_r, FR, AP duration and sag amplitude). None of the structural changes we observed in the TG cells were significantly related to any of the electrophysiological changes seen in the same cells (data not shown).

Discussion

This study was undertaken to investigate whether intracellular NFTs cause deleterious changes in the structure and function of individual layer 3 frontal cortical pyramidal cells. The frontal cortex is of particular interest in the study of tauopathies such as FTDP-17 Post-mortem examination of this area in FTDP-17 brains reveals severe cortical atrophy and a high density of neurofibrillary tangles (Wszołek

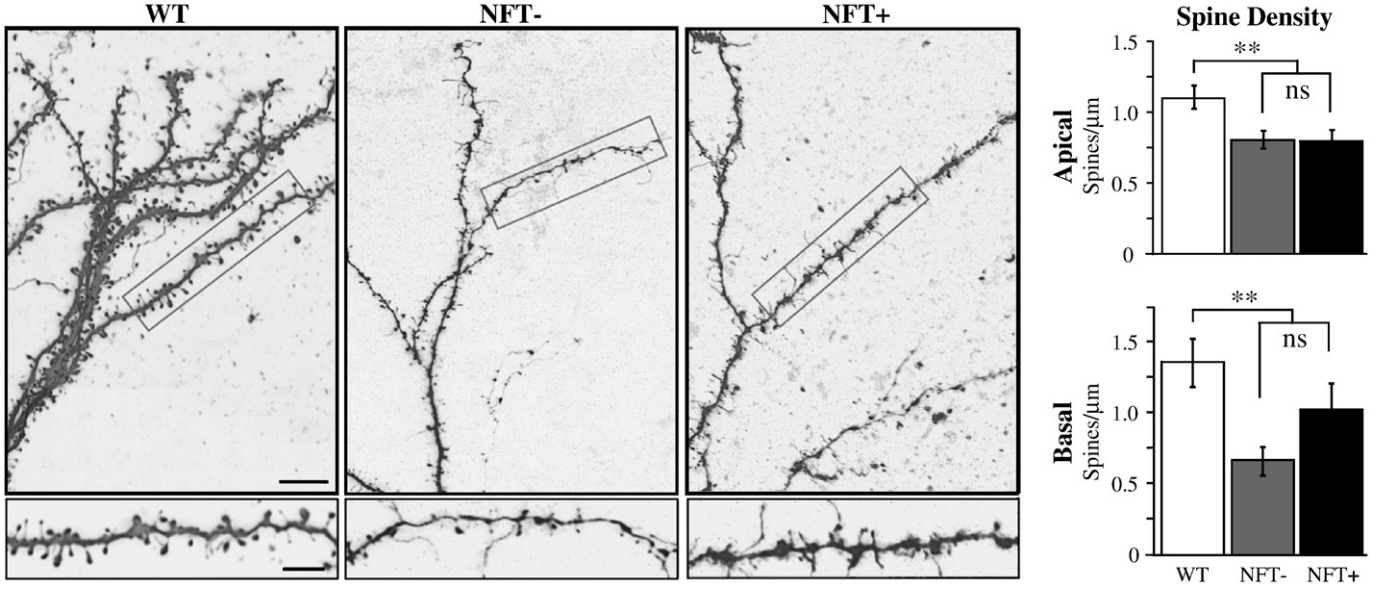

Fig. 5. Significant reduction in dendritic spine density in TG cells. Left panel, top: confocal images of apical dendritic tufts from the cells shown in Fig. 1. Bottom: higher magnification view of the boxed areas shown above. Right panel: significant reduction in spine density was observed in both the apical (top) and basal (bottom) dendritic arbors in the TG cells compared to WT. There was no difference between the NFT− and NFT+ cells within the TG group. Scale bars: top left = 10 µm; bottom left = 5 µm. **$p \leq 0.02$.

et al., 2005). These neuropathological features are also characteristic of rTg4510 mice. The present study focused on cortico-cortical layer 3 pyramidal neurons as they play a key role in the mediation of cognitive function (Morrison and Hof, 2002, 2007) which is impaired in FTDP patients. Key findings were that TG cells exhibit significantly: 1) depolarized resting membrane potentials and associated increase in AP firing rates; 2) increased amplitude depolarizing "sag" potentials; 3) truncated apical tufts; 4) reduced complexity and length of apical and basal dendritic arbors, and; 5) decreased spine density. Importantly, cells with an NFT do not differ electrophysiologically or morphologically from those with no discernable NFT. Thus, TG neurons undergo significant functional and structural alterations regardless of the presence or absence of an NFT.

Proportion of NFT− versus NFT+ neurons

Among the TG neurons examined in this study, 42% exhibited Thioflavin-S positive NFTs in their somata. The other 58% of neurons did not stain with Thioflavin-S, and hence did not contain aggregated beta-sheet fibrillar tau; however, these cells are likely to have high levels of mutated tau protein in the soluble, non-fibrillar form (Berger et al., 2007). The relatively large number of NFT+ cells seen in our study was unexpected in light of a recent study by Spires et al. (2006) which reported that ~10% of neurons in the cortex of 8 month-old rTg4510 mice contain NFTs. Spires et al. (2006) assessed NFT+ cells across laminae of multiple cortical areas (termed "cortex") while we focused exclusively on layer 3 pyramidal cells in frontal cortex; thus the difference in percentage of NFT+ cells observed in the two studies may indicate that layer 3 pyramidal cells in the frontal cortex are particularly prone to developing NFTs, as suggested by Hof (2001).

Tau expression leads to a depolarized resting membrane potential and associated increase in excitability

While input resistance and membrane time constant remain unchanged, resting membrane potential is significantly depolarized in TG cells. WT and TG cells have similar soma surface area and total cell surface area; thus it is not surprising that input resistance and membrane time constant, both functions of cell size, are not significantly different between the two cell populations. A variety of mechanisms could underlie the depolarized resting membrane potential of TG cells. First, it is plausible that the significantly increased depolarizing "sag" potential seen in TG cells could contribute, since this potential has been shown to be responsible for tonic depolarization of neurons by 4–8 mV (review: Robinson and Siegelbaum, 2003). Second, transmembrane ionic gradients and hence the resting membrane potential are maintained by a Na+/K+-ATPase pump; a reduction in the activity of this pump, such as would be seen with reduced intracellular ATP levels, will lead to depolarization of the membrane potential. In support of this idea, a significant reduction in ATP levels, reflective of mitochondrial dysfunction, has been observed in the brains of P301L transgenic mice (David et al., 2005). Third, an increase in excitatory synaptic inputs or decrease in inhibitory synaptic inputs could result in a significantly depolarized resting membrane potential in TG cells. It seems unlikely that synaptic excitation is significantly increased in TG cells given the significant loss of presynaptic glutamatergic neurons in these animals (Santacruz et al., 2005) and the reduction in the dendritic spines we observed in these cells. Inhibitory interneurons may be lost with progressive tauopathy, if so, it is plausible that there is reduced synaptic inhibition of pyramidal cells, with resulting depolarized resting membrane potential. Further studies are required to address the important question of synaptic response changes in TG cells.

The depolarized resting membrane potential of TG cells will significantly impact the integration of synaptic inputs and ultimately the functional output (in the form of action potentials) of these cells. Specifically, substantially less depolarization is required to drive TG cells to fire action potentials. Indeed, TG cells in the present study fired at significantly higher rates than did WT cells in response to identical depolarizing current steps. The implications of this excitability increase for the activity of individual neurons and networks of neurons are significant and could be viewed as potentially either detrimental or beneficial. Increased excitability could be detrimental in that the dynamic range for the modulation of the TG cells would necessarily be reduced due to a "ceiling effect" in which TG cells are closer to maximal firing rates than are WT when depolarized from rest. On the other hand, increased excitability may favor maintenance of more normal network behavior in the face of significantly reduced glutamatergic synaptic transmission within a network. Although reduced glutamatergic transmission in response to tau mutation has not been directly demonstrated to date, the extensive loss of glutamatergic presynaptic neurons and of postsynaptic dendritic spines both favor the idea that glutamatergic signalling is likely dramatically reduced. Given this, it would be advantageous that the more depolarized TG neurons require less glutamate to maintain firing rates in the normal range within a given synaptic circuit.

Significant alterations in dendritic arbors of TG cells

In the majority of TG cells (65%), there is a striking atrophy or complete loss of the apical tuft located in layer 1. In addition, apical and basal dendritic length and complexity are both significantly reduced. This is the first demonstration of major dendritic structural changes in a commonly employed mouse model of human tauopathy. The means by which these changes occur are unknown and currently under investigation, but recent studies lend insight into potential mechanisms. A number of studies have shown that mutated and/or overexpressed tau is displaced from its normal location within the axon to the somatodendritic compartment (review: Iqbal et al., 2009). This re-compartmentalization also occurs in neurodegenerative diseases such as AD (Delacourte et al., 1990), and in transgenic animal models overexpressing human tau (Andorfer et al., 2003; Hall et al., 2000). It has been demonstrated that overexpression of tau (such as occurs in rTg4510 mice) promotes dendritic cytoskeletal destabilization and disintegration as well as altered subcellular organelle trafficking (Hall et al., 2000), either of which could substantially contribute to the dendritic alterations observed in the TG cells in the present study. This is the first study to examine the detailed morphology of cortical pyramidal neurons in P301L mutant mice. However, an earlier study reported a modest increase in the mean length of the terminal branches of CA1 pyramidal cell apical dendrites in very young P301L mutant mice (Boekhoorn et al., 2006). Thus, tau mutation can lead to either a lengthening or reduction in dendritic extent depending upon the cell type examined or possibly the age of the experimental subjects. The difference in findings could also plausibly be explained by differences in the tau isoform expressed by the mutant mice (4R2N versus 4R0N) or in the methodology employed (Golgi impregnation and light microscopy versus intracellular filling and confocal microscopy).

The dendritic architecture changes we have demonstrated are likely to impact dendritic integration of synaptic inputs; in particular the loss of the apical tuft would be expected to have a major impact on synaptic integration by these neurons because the tuft is the principal recipient of monoaminergic modulatory influences (Thierry et al., 1990), thalamic inputs (van Groen et al., 1999), and feedback intracortical connections (Rockland and Pandya, 1979). Because inputs to the apical tuft are dense, diverse and complex, it is difficult to predict with precision what the physiological impact of loss of this extensive postsynaptic area would be, other than that it would likely be consequential with regard to the synaptic integration by individual neurons and to network properties. The loss of the apical tuft highlights the need for further studies examining both spontaneous and evoked synaptic response properties of TG neurons.

Dramatic and uniform decrease in spine density in TG cells

This is the first demonstration that expression of mutant tau results in a significant loss of dendritic spines in cortical pyramidal cells. The 29–38% reduction in the dendritic spine density we observed is reminiscent of the 37–41% reduction in density of synaptophysin labeling reported in the prefrontal cortex of FTD patients (Liu et al., 1996). Similarly, investigations performed in other transgenic mouse models expressing mutated tau have demonstrated reduced numbers of dendritic spines (Mocanu et al., 2008) and synaptophysin labeling (Schindowski et al., 2006) in the hippocampus. Thus, there is accumulating evidence that tau mutations can result in significant loss of dendritic spines. Understanding the mechanisms by which tau alterations induce loss of dendritic spines is a rich and important area for future research.

Conclusions

Perhaps the most unexpected finding of the present study was that major structural and functional changes occur in TG neurons *regardless* of the presence or absence of NFTs and that some NFT+ and some NFT− cells are indistinguishable from WT cells with regard to both structure and function. These findings provide strong and direct support for the idea that NFTs *per se* are not necessarily toxic to neurons and that non-fibrillar tau species, undetectable by Thioflavin-S, can have significant detrimental effects on the structure and function of neurons.

Acknowledgments

Supported by NIH/NIA P30 AG13846 and R01 AG025062 (J. Luebke); NIH/NINDS R01 NS046355 and Alzheimer's Association IIRG-06-27277 (J. Lewis). We thank Dr. Benjamin Wolozin for helpful comments on the manuscript, and Drs. Susan Wearne and Patrick Hof for helpful comments and technical advice on spine analyses. J. Lewis and Mayo Clinic hold the patent associated with the rTg4510 mice, have a financial interest associated with the rTg4510 mice and have received annual royalties from the licensing of the first technology of greater than the federal threshold for significant financial interest.

References

Andorfer, C., Acker, C.M., Kress, Y., Hof, P.R., Duff, K., Davies, P., 2005. Cell-cycle reentry and cell death in transgenic mice expressing nonmutant human tau isoforms. J. Neurosci. 25, 5446–5454.

Andorfer, C., Kress, Y., Espinoza, M., de Silva, R., Tucker, K.L., Barde, Y.A., Duff, K., Davies, P., 2003. Hyperphosphorylation and aggregation of tau in mice expressing normal human tau isoforms. J. Neurochem. 86, 582–590.

Ballatore, C., Lee, V.M., Trojanowski, J.Q., 2007. Tau-mediated neurodegeneration in Alzheimer's disease and related disorders. Nat. Rev. Neurosci. 8, 663–672.

Berger, Z., Roder, H., Hanna, A., Carlson, A., Rangachari, V., Yue, M., Wszolek, Z., Ashe, K., Knight, J., Dickson, D., Andorfer, C., Rosenberry, T.L., Lewis, J., Hutton, M., Janus, C., 2007. Accumulation of pathological tau species and memory loss in a conditional model of tauopathy. J. Neurosci. 27, 3650–3662.

Boekhoorn, K., Terwel, D., Biemans, B., Borghgraef, P., Wiegert, O., Ramakers, G.J., de Vos, K., Krugers, H., Tomiyama, T., Mori, H., Joels, M., van Leuven, F., Lucassen, P.J., 2006. Improved long-term potentiation and memory in young tau-P301L transgenic mice before onset of hyperphosphorylation and tauopathy. J. Neurosci. 26, 3514–3523.

Bretteville, A., Planel, E., 2008. Tau aggregates: toxic, inert, or protective species? J. Alzheimers Dis. 14, 431–436.

Bussière, T., Gold, G., Kövari, E., Giannakopoulos, P., Bouras, C., Perl, D.P., Morrison, J.H., Hof, P.R, 2003. Stereologic analysis of neurofibrillary tangle formation in prefrontal cortex area 9 in aging and Alzheimer's disease. Neuroscience 117, 577–592.

Chang, Y.M., Luebke, J.I., 2007. Electrophysiological diversity of layer 5 pyramidal cells in the prefrontal cortex of the rhesus monkey: in vitro slice studies. J. Neurophysiol. 98, 2622–2632.

Chang, Y.M., Rosene, D.L., Killiany, R.J., Mangiamele, L.A., Luebke, J.I., 2005. Increased action potential firing rates of layer 2/3 pyramidal cells in the prefrontal cortex are significantly related to cognitive performance in aged monkeys. Cereb. Cortex 15, 409–418.

Congdon, E.E., Duff, K.E., 2008. Is tau aggregation toxic or protective? J. Alzheimers. Dis. 14, 453–457.

David, D.C., Hauptmann, S., Scherping, I., Schuessel, K., Keil, U., Rizzu, P., Ravid, R., Drose, S., Brandt, U., Muller, W.E., Eckert, A., Gotz, J., 2005. Proteomic and functional analyses reveal a mitochondrial dysfunction in P301L tau transgenic mice. J. Biol. Chem. 280, 23802–23814.

Delacourte, A., Flament, S., Dibe, E.M., Hublau, P., Sablonniere, B., Hemon, B., Sherrer, V., Defossez, A., 1990. Pathological proteins Tau 64 and 69 are specifically expressed in the somatodendritic domain of the degenerating cortical neurons during Alzheimer's disease. Demonstration with a panel of antibodies against Tau proteins. Acta Neuropathol. 80, 111–117.

Hall, GF, Chu, B, Lee, G, Yao, J, 2000. Human tau filaments induce microtubule and synapse loss in an in vivo model of neurofibrillary degenerative disease. J. Cell. Sci. 113, 1373–1387.

Hof, P.R., 2001. Alzheimer's disease. In: Hof, P.R., Mobbs, C.V. (Eds.), Functional Neurobiology of Aging. Academic Press, San Diego, pp. 95–127.

Iqbal, K., Liu, F., Gong, C.X., Alonso, A.D., Grundke-Iqbal, I., 2009. Mechanisms of tau-induced neurodegeneration. Acta Neuropathol. 118, 53–69.

Lee, V.M., Goedert, M., Trojanowski, J.Q., 2001. Neurodegenerative tauopathies. Annu. Rev. Neurosci. 24, 1121–1159.

Lewis, J., Hutton, M., 2005. Animal models of tauopathies. In: Litvan, I. (Ed.), Atypical Parkinsonian Disorders. Humana Press, New York, pp. 65–76.

Liu, X., Erikson, C., Brun, A., 1996. Cortical synaptic changes and gliosis in normal aging, Alzheimer's disease and frontal lobe degeneration. Dementia 7, 128–134.

Mocanu, M.M., Nissen, A., Eckermann, K., Khlistunova, I., Biernat, J., Drexler, D., Petrova, O., Schonig, K., Bujard, H., Mandelkow, E., Zhou, L., Rune, G., Mandelkow, E.M., 2008. The potential for beta-structure in the repeat domain of tau protein determines aggregation, synaptic decay, neuronal loss, and coassembly with endogenous Tau in inducible mouse models of tauopathy. J. Neurosci. 28, 737–748.

Morrison, J.H., Hof, P.R., 2002. Selective vulnerability of corticocortical and hippocampal circuits in aging and Alzheimer's disease. Prog. Brain Res. 136, 467–486.

Morrison, J.H., Hof, P.R., 2007. Life and death of neurons in the aging cerebral cortex. Int. Rev. Neurobiol. 81, 41–57.

Poorkaj, P., Grossman, M., Steinbart, E., Payami, H., Sadovnick, A., Nochlin, D., Tabira, T., Trojanowski, J.Q., Borson, S., Galasko, D., Reich, S., Quinn, B., Schellenberg, G., Bird, T.D., 2001. Frequency of tau gene mutations in familial and sporadic cases of non-Alzheimer dementia. Arch. Neurol. 58, 383–387.

Radley, J.J., Rocher, A.B., Rodriguez, A., Ehlenberger, D.B., Dammann, M., McEwen, B.S., Morrison, J.H., Wearne, S.L., Hof, P.R., 2008. Repeated stress alters dendritic spine morphology in the rat medial prefrontal cortex. J. Comp. Neurol. 507, 1141–1150.

Robinson, R.B., Siegelbaum, S.A., 2003. Hyperpolarization-activated cation currents: from molecules to physiological function. Annu. Rev. Physiol. 65, 453–480.

Rockland, K.S., Pandya, D.N., 1979. Laminar origins and terminations of cortical connections of the occipital lobe in the rhesus monkey. Brain Res. 179, 3–20.

Rodriguez, A., Ehlenberger, D., Kelliher, K., Einstein, M., Henderson, S.C., Morrison, J.H., Hof, P.R., Wearne, S.L., 2003. Automated reconstruction of three-dimensional neuronal morphology from laser scanning microscopy images. Methods 30, 94–105.

Rodriguez, A., Ehlenberger, D.B., Hof, P.R., Wearne, S.L., 2006. Rayburst sampling, an algorithm for automated three-dimensional shape analysis from laser scanning microscopy images. Nat. Protoc. 1, 2152–2161.

Santa-Maria, I., Perez, M., Hernandez, F., Avila, J., Moreno, F.J., 2006. Characteristics of the binding of thioflavin S to tau paired helical filaments. J. Alzheimers Dis. 9, 279–285.

Santacruz, K., Lewis, J., Spires, T., Paulson, J., Kotilinek, L., Ingelsson, M., Guimaraes, A., DeTure, M., Ramsden, M., McGowan, E., Forster, C., Yue, M., Orne, J., Janus, C., Mariash, A., Kuskowski, M., Hyman, B., Hutton, M., Ashe, K.H., 2005. Tau suppression in a neurodegenerative mouse model improves memory function. Science 309, 476–481.

Schindowski, K., Bretteville, A., Leroy, K., Begard, S., Brion, J.P., Hamdane, M., Buee, L., 2006. Alzheimer's disease-like tau neuropathology leads to memory deficits and loss of functional synapses in a novel mutated tau transgenic mouse without any motor deficits. Am. J. Pathol. 169, 599–616.

Sholl, D.A., 1953. Dendritic organization in the neurons of the visual and motor cortices of the cat. J. Anat. 87, 387–406.

Spires-Jones, T.L., Stoothoff, W.H., de Calignon, A., Jones, P.B., Hyman, B.T., 2009. Tau pathophysiology in neurodegeneration: a tangled issue. Trends Neurosci. 32, 150–159.

Spires, T.L., Orne, J.D., SantaCruz, K., Pitstick, R., Carlson, G.A., Ashe, K.H., Hyman, B.T., 2006. Region-specific dissociation of neuronal loss and neurofibrillary pathology in a mouse model of tauopathy. Am. J. Pathol. 168, 1598–1607.

Sun, A., Nguyen, X.V., Bing, G., 2002. Comparative analysis of an improved thioflavin-S stain, Gallyas silver stain, and immunohistochemistry for neurofibrillary tangle demonstration on the same sections. J. Histochem. Cytochem. 50, 463–472.

Thierry, A.M., Godbout, R., Mantz, J., Glowinski, J., 1990. Influence of the ascending monoaminergic systems on the activity of the rat prefrontal cortex. Prog. Brain Res. 85, 357–364 discussion, 364–355.

van Groen, T., Kadish, I., Wyss, J.M., 1999. Efferent connections of the anteromedial nucleus of the thalamus of the rat. Brain Res. Brain Res. Rev. 30, 1–26.

Wearne, S.L., Rodriguez, A., Ehlenberger, D.B., Rocher, A.B., Henderson, S.C., Hof, P.R., 2005. New techniques for imaging, digitization and analysis of three-dimensional neural morphology on multiple scales. Neuroscience 136, 661–680.

Wszołek, Z.K., Słowiński, J., Golan, M., Dickson, D.W, 2005. Frontotemporal dementia and parkinsonism linked to chromosome 17. Folia Neuropathol. 43, 258–270.

Zhang, K., Peng, B.W., Sanchez, R.M., 2006. Decreased I_H in hippocampal area CA1 pyramidal neurons after perinatal seizure-inducing hypoxia. Epilepsia 47, 1023–1028.